Electronic Supplementary Information

Cu-modified electrolyte-gated transistors based on reduced graphene oxide

Rafael Cintra Hensel[1], Nicola Comisso[2], Marco Musiani[2], Francesco Sedona[1], Mauro Sambi[1], Nicolò Lago[3], Andrea Cester[3], Stefano Casalini[1,*].

[1]Department of Chemical Sciences (DiSC), University of Padua, via Marzolo 1, 35131, Padua (Italy)

[2]Institute of Condensed Matter Chemistry and Technologies for Energy (ICMATE), National Research Council (CNR), Corso Stati Uniti 4, 35127, Padua (Italy)

[3]Department of Information Engineering (DEI), University of Padua, via Gradenigo 6/b, 35131, Padua (Italy)

Hydrogen bubble templated cathodic electrodeposition of metals.

***Essential features*:** To obtain Cu deposits with a much larger surface area, we exploited the hydrogen bubble dynamic template cathodic deposition approach which has been described by various authors for Cu and some other metals [1-10]. In this approach, the electrodeposition is normally performed by imposing cathodic currents times higher than the limiting diffusion current of the metal ion that undergoes reduction. Under these conditions, electrochemical reduction of H^+ (or water), to generate molecular H_2, occurs in parallel with metal deposition, molecular hydrogen saturates the solution next to the cathode surface forming tiny H_2 bubbles that adhere to the electrode for a certain lapse of time before being released. Thus, the metal deposit grows around the H_2 bubbles and being deposited under diffusion control, tends to form nanowires or dendrites. The bubbles release stirs the solution and interrupts the growth of large and fragile dendrites (typical of deposition processes occurring under diffusion control), while new growth centres are nucleated. When the electrolysis is stopped, the dynamic template formed by hydrogen bubbles spontaneously disappears, leaving metal deposits with a bimodal porosity, with larger pores a few tens of microns wide, due to bubbles, and much tinier voids between nanowires. Such porous deposits exhibit good mechanical resistance. By using hydrogen bubble dynamic template cathodic deposition, Cu and Cu alloy deposits with surface roughness factors, *i.e.* ratios between true and geometric surface areas, well above 100 could be easily obtained on disc or sheet electrodes [11].

***Peculiarities of hydrogen bubble-assisted deposition onto Au thin-layer gates*:** A major requirement for the successful electrodeposition of porous metal layers is the use of a high cathodic current density. This is normally not a problem when solid metal electrodes (rods or sheets) are used. However, the electrical connection to the Au gate was ensured by an Au lead 0.1 cm wide and 20 nm

thick (section area of the conducting lead $2x10^{-7}$ cm^2). Thus, by selecting a current of 0.09 A for the gate with an area equal to 0.09 cm^2 (to achieve a current density of 1.0 A cm^{-2}, typically used in the deposition of porous metals) the current density across the vertical section of the lead was equal to 450 kA cm^{-2}. This high current density caused a marked and spatially confined heating of the Au lead, which induced partial or complete delamination of the Au lead from the underlying PET substrate. By depositing a compact and relatively thick Cu layer on the Au lead, ahead of the porous Cu deposition, the overall thickness of the gate terminal was increased by a large factor, and the current density in the lead was correspondingly decreased to ca. 2.4 kA cm^{-2}. Under these conditions, no detachment of Au from PET was observed, and porous Cu layers could be obtained.

Figures S1-S3 – Morphological characteristics of the electrodeposited Cu.

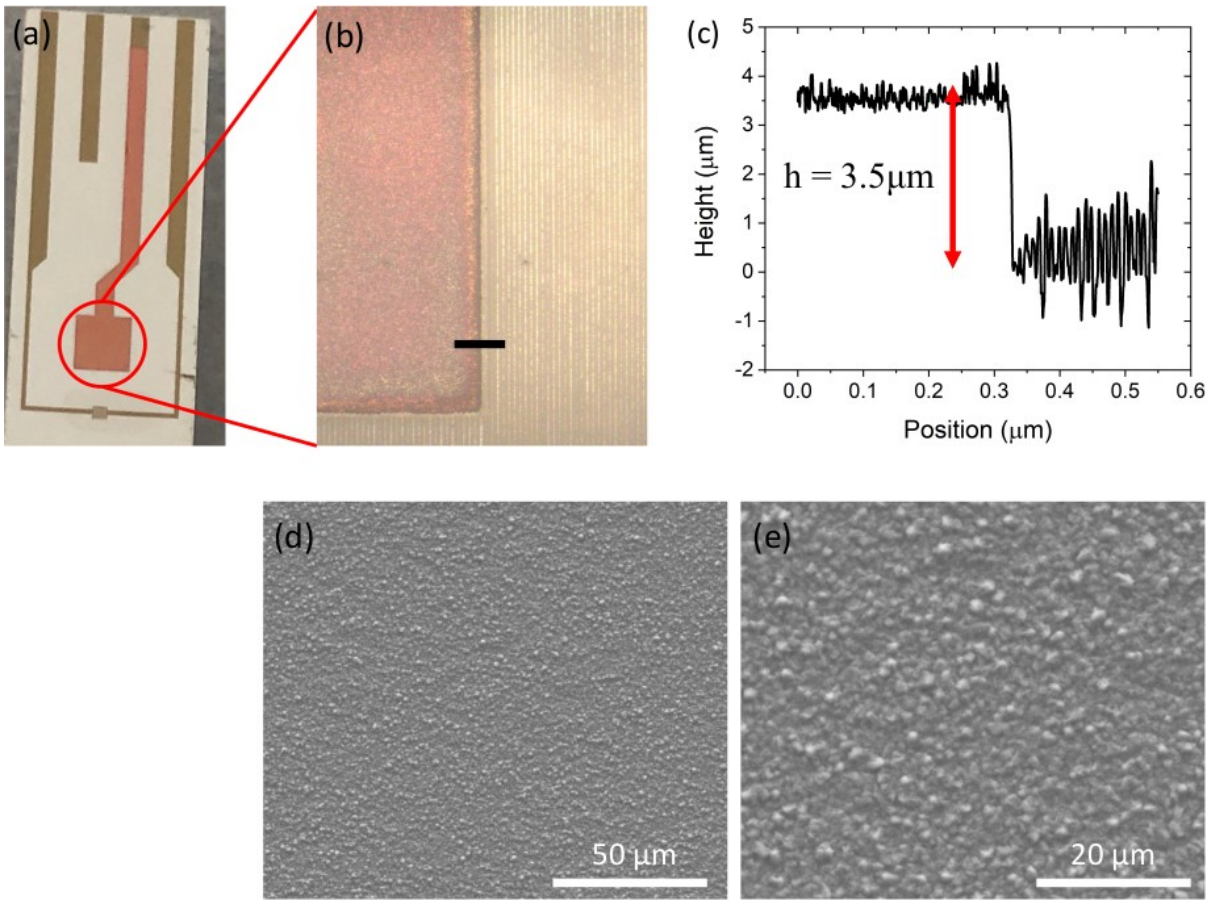

Figure S1: (a) Picture of the cCu-gated device; (b) optical image of the cCu gate; (c) height profile corresponding to the black line indicated in (b); (d,e) SEM micrographs of the cCu for different magnifications.

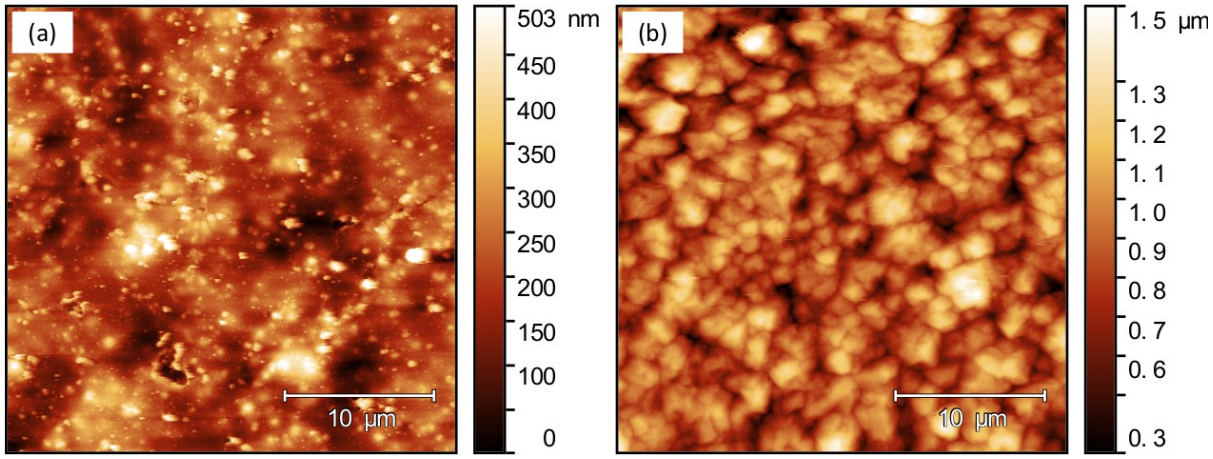

Figure S2: AFM images of the (a) pristine Au and (b) cCu coating.

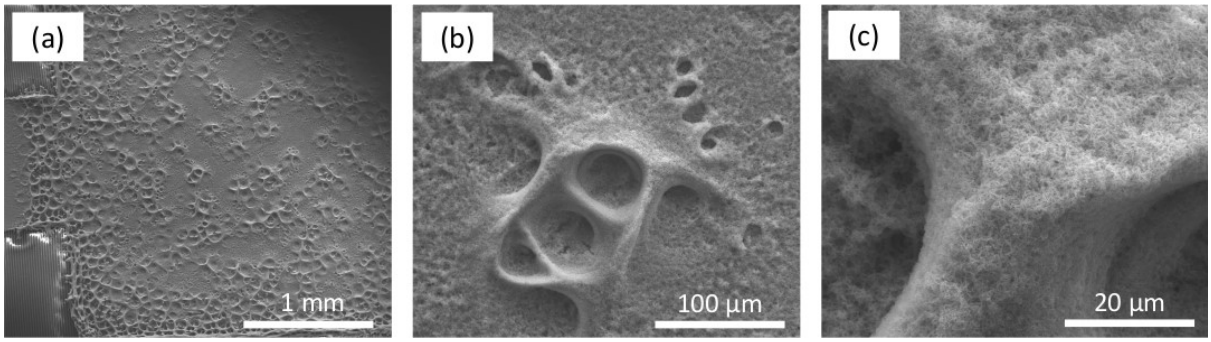

Figure S3: SEM micrographs of the pCu for different magnifications.

Figures S4-S5, Table S1 and relevant comments – I-V transfer characteristics

The I-V transfer characteristics in 0.1 M NaCl show a quite weak shift of minimum gate voltage, $V_{G,min}$, for the pristine Au-gated devices. On the contrary, both cCu and pCu present a clear shift of the $V_{G,min}$ when operated in the same conditions, as shown in Figure S4b-c, respectively. Furthermore, n-type conduction dominates for both Cu-modified gates. The mobility of holes (μ_h) and electrons (μ_e) was calculated by using the equations that describe ambipolar transistors (Equation S1). The obtained mobility values, threshold voltages and minimum gate voltage are presented in Table S1. For the pristine Au-gated device, only the mobility of holes μ_h was obtained due to the high mean threshold voltage of the n-type charge carriers ($V_{Th,N}$) that is out of our measuring range. Analogously, only the electron mobility μ_e was obtained for cCu-gated device in 0.1M NaCl.

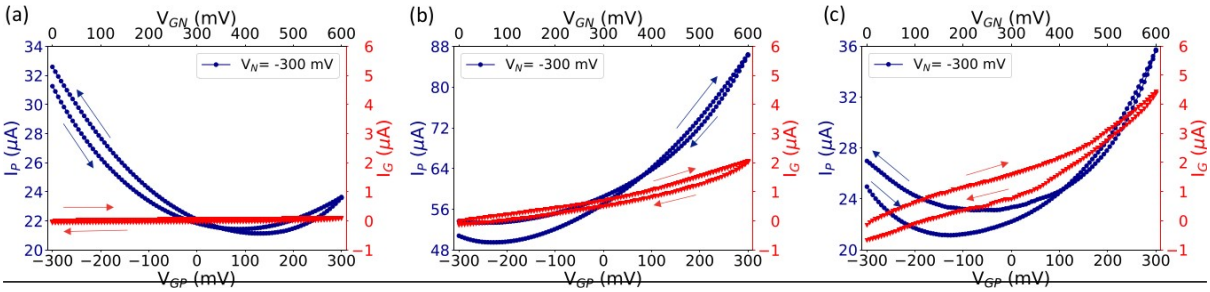

Figure S4: I-V transfer characteristics of rGO device featuring (a) pristine Au, (b) cCu-coated Au gate, (c) pCu-coated Au gate in NaCl 0.1M. The red curve stands for the leakage current (I_G) and the blue one stands for the current recorded at the P terminal (I_P). V_P = 0 V and V_N = -300 mV.

$$I_{PN_{FET}} = \frac{W}{L} C_i \cdot \begin{cases} \dfrac{\mu_{0p}}{(2+\alpha_p)V_{0p}^{\alpha_p}}\left[(V_G - V_{Tp} - V_P)^{2+\alpha_p} - (V_G - V_{Tp} - V_N)^{2+\alpha_p}\right] & Linear\ (type\ P) \\ \dfrac{\mu_{0p}}{(2+\alpha_p)V_{0p}^{\alpha_p}}(V_G - V_{Tp} - V_P)^{2+\alpha_p} & Saturation\ (type\ P) \\ \left[\dfrac{\mu_{0p}}{(2+\alpha_p)V_{0p}^{\alpha_p}}(V_G - V_{Tp} - V_P)^{2+\alpha_p} + \dfrac{\mu_{0n}}{(2+\alpha_n)V_{0n}^{\alpha_n}}(V_G - V_{Tn} - V_N)^{2+\alpha_n}\right] & Ambipolar \\ \dfrac{\mu_{0n}}{(2+\alpha_n)V_{0n}^{\alpha_n}}(V_G - V_{Tn} - V_N)^{2+\alpha_n} & Saturation\ (type\ N) \\ \dfrac{\mu_{0n}}{(2+\alpha_n)V_{0n}^{\alpha_n}}\left[(V_G - V_{Tn} - V_N)^{2+\alpha_n} - (V_G - V_{Tn} - V_P)^{2+\alpha_n}\right] & Linear\ (type\ N) \end{cases} \quad (Equation\ S1)$$

In equation S1, V_{TP} and V_{TN} are the p- and n-type threshold voltages, α_P and α_N are the p- and n-type mobilities enhancement factors were extracted from $I^*_{PN_{FET}}$ in unipolar saturation regimes (p- and n-type respectively). C_i = 5 μF cm^{-2} was assumed, according to ref [12].

Table S1: Threshold voltage for holes ($V_{Th,P}$) and electrons ($V_{Th,N}$), field-effect mobility (μ) and minimum gate voltage ($V_{G,min}$) calculated according to the data shown in Figure 1 and Figure S4 for each gate composition and porosity in Milli-Q water and 0.1 M NaCl considering both the forward and the reverse scan. Missing vales corresponds to missing n- or p- branches of the IV transfer characteristics.

		$V_{Th,P}$ (mV)	μ_h ($cm^2V^{-1}s^{-1}$)	$V_{Th,N}$ (mV)	μ_e ($cm^2V^{-1}s^{-1}$)	$V_{G,min}$ (mV)
Au in water	forward scan	162 ± 7	0.11 ± 0.01	284 ± 12	-	126 ± 5
	reverse scan	184 ± 3	0.10 ± 0.01	401 ± 10	-	139 ± 5
Au in NaCl	forward scan	188 ± 5	0.12 ± 0.01	344 ± 8	-	150 ± 5
	reverse scan	171 ± 2	0.09 ± 0.01	383 ± 10	-	105 ± 5
cCu in water	forward scan	89 ± 3	0.12 ± 0.01	303 ± 9	0.07 ± 0.01	55 ± 5
	reverse scan	121 ± 5	0.05 ± 0.01	346 ± 6	0.11 ± 0.03	71 ± 5
cCu in NaCl	forward scan	-145 ± 60	-	46 ± 1	0.2 ± 0.1	-148 ± 12
	reverse scan	-167 ± 90	-	6 ± 8	0.10 ± 0.01	-242 ± 50
pCu in water	forward scan	36 ± 13	0.16 ± 0.01	202 ± 9	0.10 ± 0.01	-19 ± 5
	reverse scan	102 ± 18	0.067 ± 0.001	344 ± 6	0.012 ± 0.001	93 ± 10
pCu in NaCl	forward scan	-60 ± 13	1.10 ± 0.01	135 ± 22	0.09 ± 0.01	-68 ± 10
	reverse scan	49 ± 26	0.42 ± 0.01	127 ± 63	0.19 ± 0.01	-21 ± 10

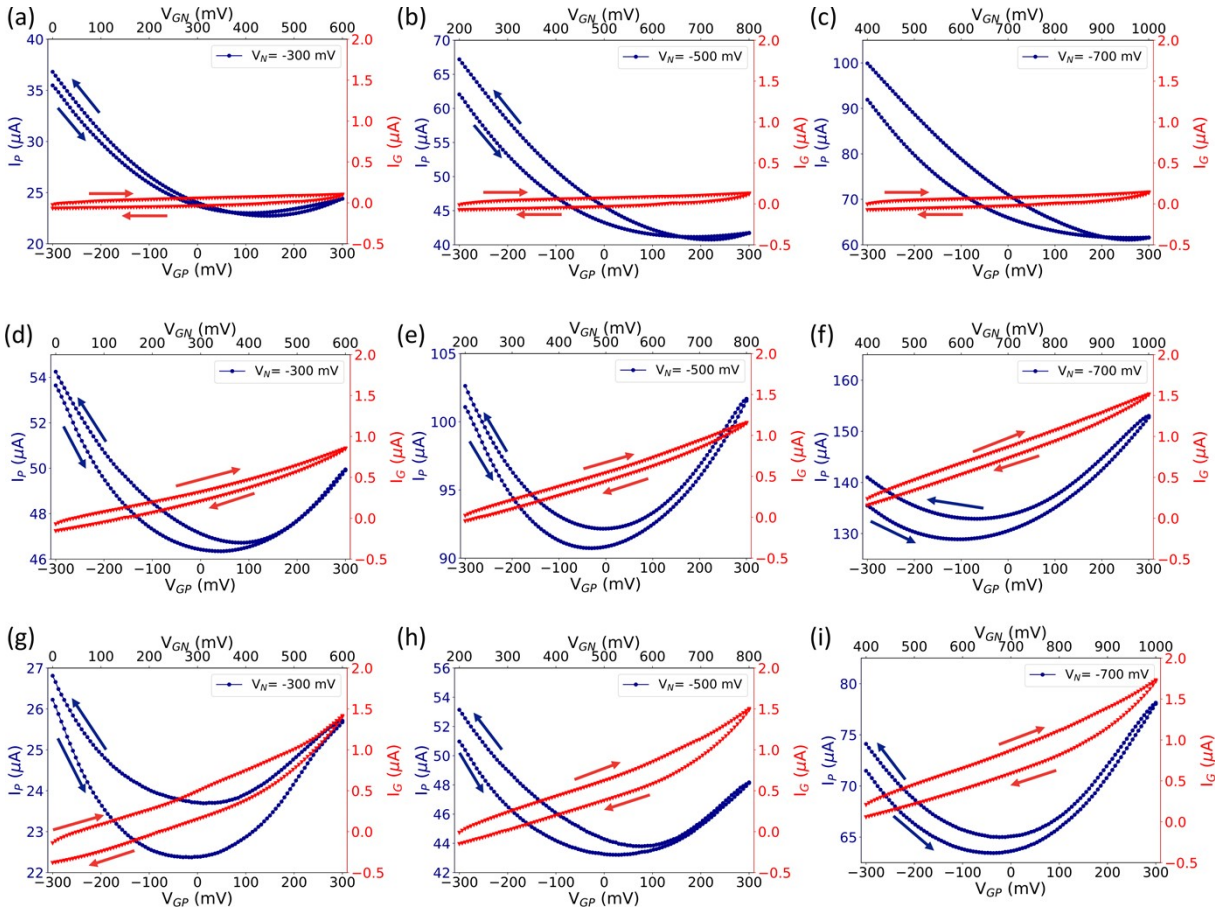

Figure S5: I-V transfer characterization of rGO device having (a-c) Au, (d,f) cCu, (g,i) pCu gate in Milli-Q water for (a,d,g) V_N = -300 mV, (b,e,h) V_N = -500 mV, (c,f,i) V_N = -700 mV. The red curve

stands for the leakage current (I_G) and the blue one stands for the current recorded at the P terminal (I_P) for $V_P = 0$ V.

Figures S6-S8, Table S2 – Transient phenomena

Figure S6 and Figure S7 respectively present the response time and the potentiometric sensitivity of the Cu-gated devices. The figures of merit of these devices are summarized in Table S2.

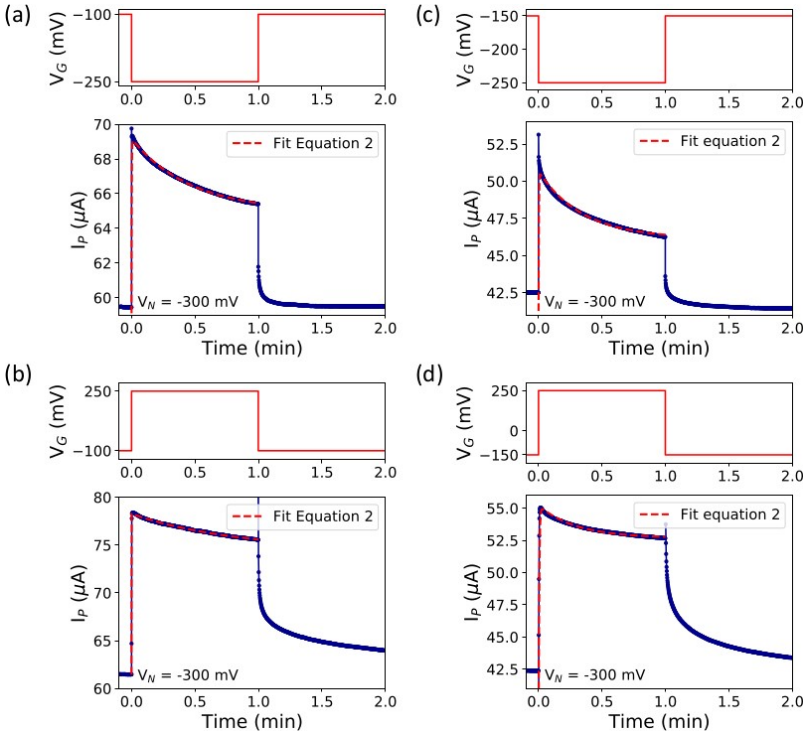

Figure S6: Response time of (a-b) cCu and (c-d) pCu devices in 0.1M NaCl when switching from the neutrality point to (a,c) p-type conduction / (b,d) n-type conduction, and then returning to the neutrality point.

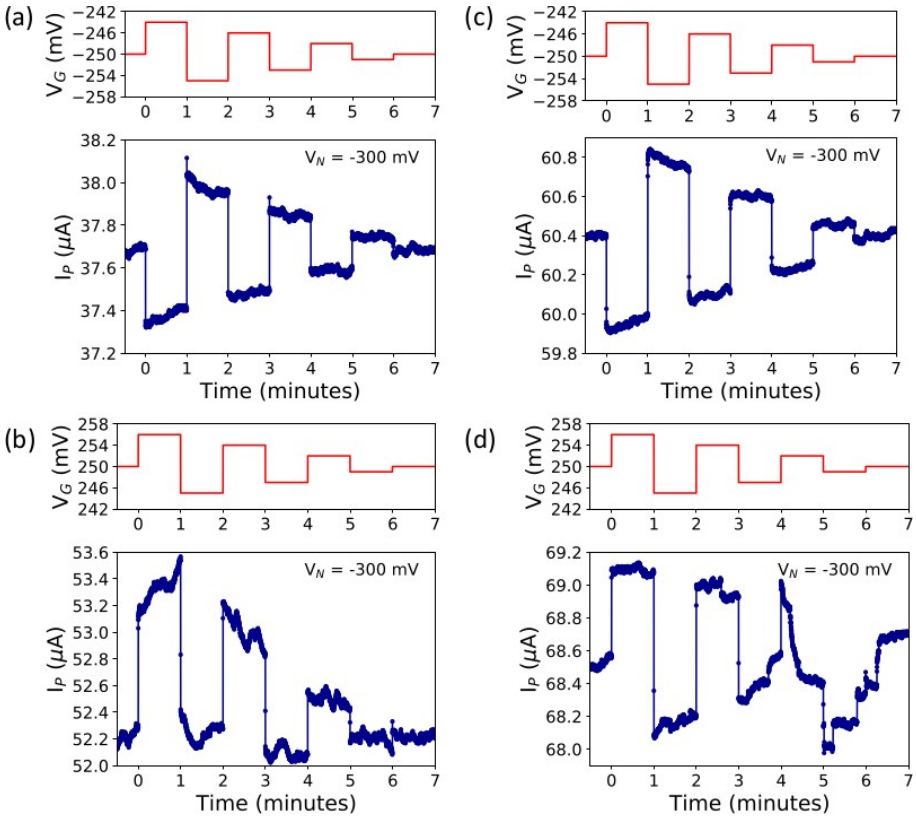

Figure S7: Potentiometric sensitivity of the (a-b) pCu-gated and (c-d) c-Cu EGOFET subjected to a train of pulses (a,c) V_{GP} = -250, -244, -255, -246, -253, -248, -251, -250 mV, (b,d) V_{GP} = +250, +256, +245, +254, +247, +252, +249, +250 mV in 0.1M NaCl.

Table S2: Figure of merits of the Au, cCu, and pCu-gated devices in which p-type corresponds to V_G = -250 mV and n-type to V_G = +250 mV; SNR, S = stored, and D = delivered.

	τ_1 (s)	τ_2 (s)	ΔV_{min} (mV)	ΔV_{min} SNR	P_D (μW.cm^{-2})	E_D (μWh.cm^{-2})	E_s/E_D
Au p-type	9.5	0.06	1	1.4	-	-	-
cCu p-type	28	0.10	1	4	-	-	-
cCu n-type	49	0.03	7	0.2	57	0.001	1.6%
pCu p-type	26	0.08	1	5.8	-	-	-
pCu n-type	26	0.09	3	12	84	0.003	3.5%

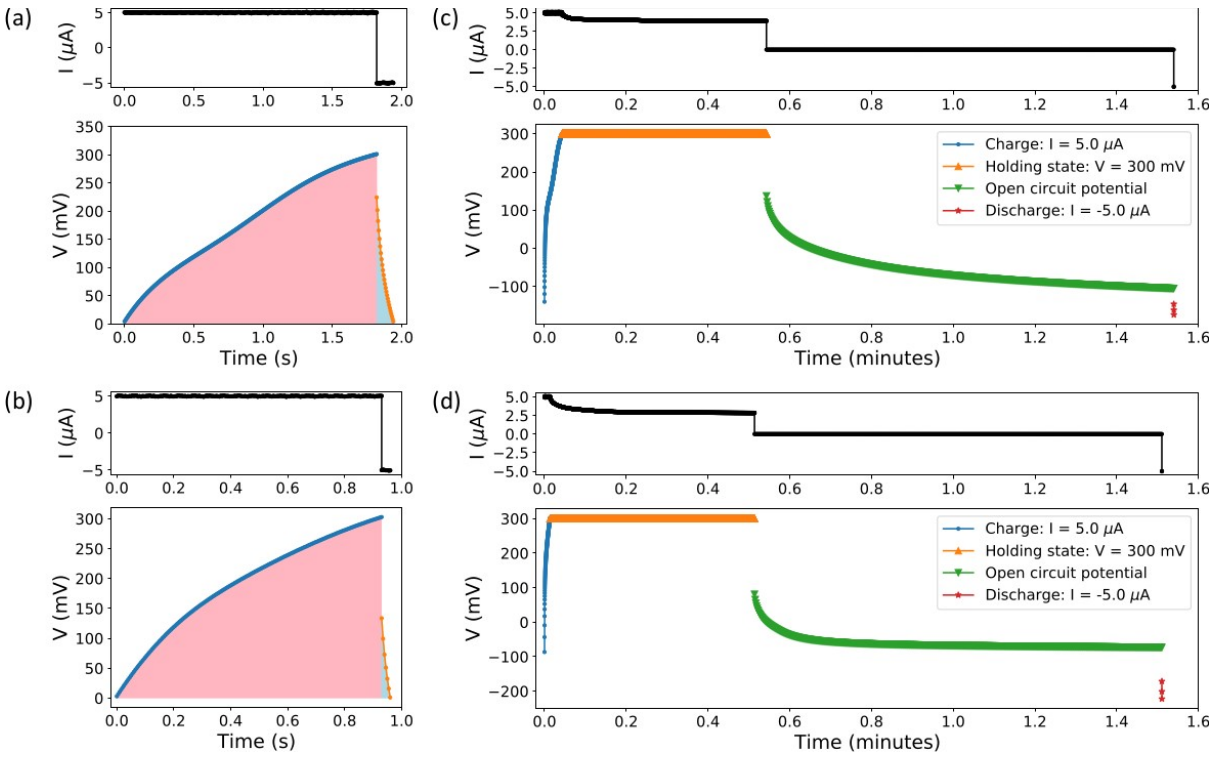

Figure S8: Galvanostatic charge/discharge for (a) pCu and (b) cCu-gated devices fixing I_{charge} = 5 µA, $I_{discharge}$ = -5 µA. Galvanostatic charge/discharge including a holding state maintaining V_{GP} = 300 mV for 30 s, and an OCP step for 60 s between the charge/discharge cycle for (c) pCu and (d) cCu-gated devices. Measurements were performed in 0.1 M NaCl.

Figures S9-S12 - emulated action potential and prolonged electrical stress

A single eAP is shown in Figure S9, whose potential setpoint is equal to + 250 mV and -250 mV. For the cCu-gated device biased at +250 mV, it was possible to record properly such an electrical stimulus (Figure S10a). Unfortunately, the cCu-gate device failed to record the same eAP featuring a potential setpoint equal to -250 mV, as expected from the potentiometric sensitivity (Figure S4b) previously described.

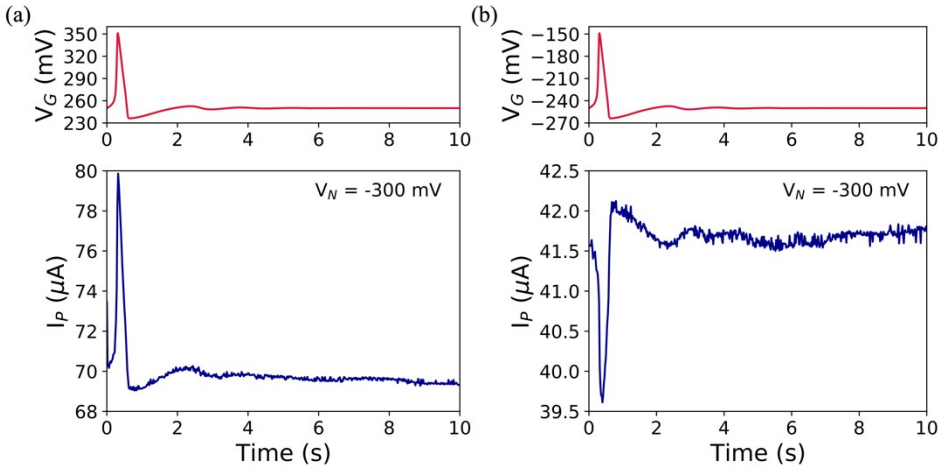

Figure S9: Upper panels: eAPs featuring a voltage setpoint equal to +250 mV and b) -250 mV. Lower panels: corresponding I_P-time recordings with V_N = -300 mV for the pCu-gated device.

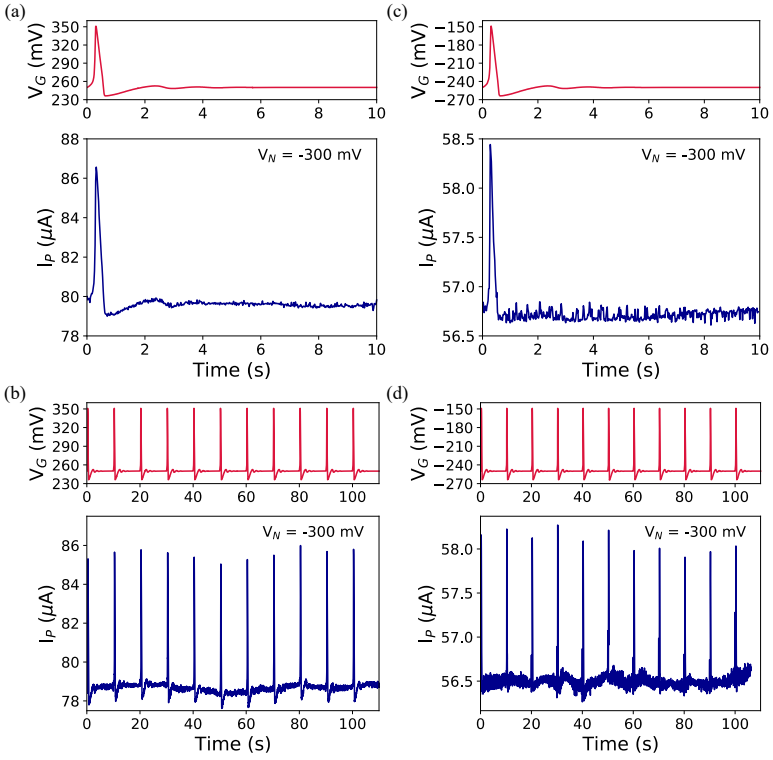

Figure S10: (a,c-top) eAPs and (a-bottom) their recordings for V_N = -300 mV; (b,d-top) eAPs and (b-bottom) their recordings for V_N = -300 mV for the cCu-gated device.

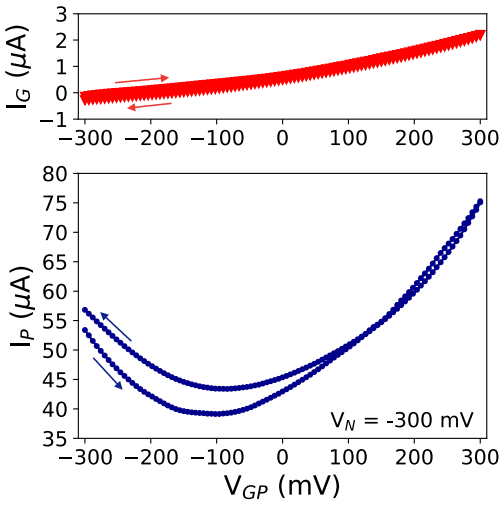

Figure S11: I-V transfer characteristics of rGO device featuring pCu-coated Au gate in 0.1 M NaCl after the fluidics measurement. The top panel stands for the leakage current (I_G) and the bottom one stands for the current recorded at the P terminal (I_P).

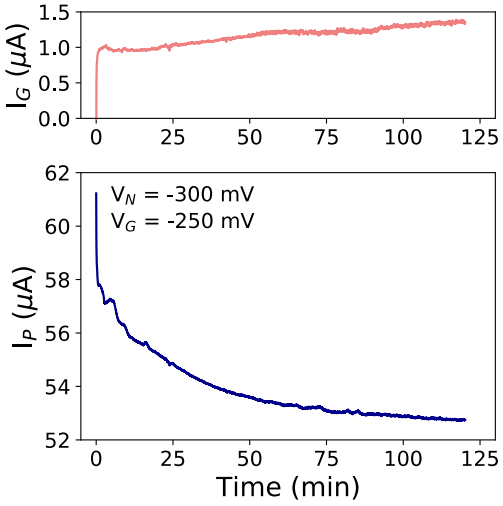

Figure S12: I_P current recorded for 2h of 0.1M NaCl flux by means of the fluidics paper for V_N = -300 mV and V_{GP} = -250 mV using the cCu-gated device.

References

[1] H.-C. Shin, J. Dong and M. Liu, *Advanced Materials*, 2003, **15**, 1610–1614.
[2] H.-C. Shin and M. Liu, *Chemistry of Materials*, 2004, **16**, 5460–5464.
[3] N. D. Nikolić and K. I. Popov, in *Electrodeposition: Theory and Practice*, ed. S. S. Djokic, Springer New York, New York, NY, 2010, pp. 1–70.
[4] Y. Li, W.-Z. Jia, Y.-Y. Song and X.-H. Xia, *Chemistry of Materials*, 2007, **19**, 5758–5764.
[5] D. Nam, R. Kim, D. Han, J. Kim and H. Kwon, *Electrochim Acta*, 2011, **56**, 9397–9405.
[6] S. Cherevko, X. Xing and C.-H. Chung, *Electrochem commun*, 2010, **12**, 467–470.
[7] S. Cherevko and C.-H. Chung, *Electrochim Acta*, 2010, **55**, 6383–6390.
[8] S. Cherevko and C.-H. Chung, *Electrochem commun*, 2011, **13**, 16–19.
[9] S. Cherevko, X. Xing and C.-H. Chung, *Appl Surf Sci*, 2011, **257**, 8054–8061.
[10] L. Mattarozzi, S. Cattarin, N. Comisso, P. Guerriero, M. Musiani and E. Verlato, *Electrochim Acta*, 2016, **198**, 296–303.
[11] N. Comisso, S. Cattarin, P. Guerriero, L. Mattarozzi, M. Musiani, L. Vázquez-Gómez and E. Verlato, *Journal of Solid State Electrochemistry*, 2016, **20**, 1139–1148.
[12] R. Furlan de Oliveira, P. A. Livio, V. Montes-García, S. Ippolito, M. Eredia, P. Fanjul-Bolado, M. B. González García, S. Casalini and P. Samorì, *Adv Funct Mater*, 2019, **29**, 1905375.